Aerocapture Guidance and Performance at Mars for High-Mass Systems

Carlie H. Zumwalt*, Ronald R. Sostaric†, and Carlos H. Westhelle‡
NASA Johnson Space Center, Houston, Texas, 77058, USA

Alicia Dwyer Cianciolo§
NASA Langley Research Center, Hampton, VA, 23681, USA

The objective of this study is to understand the performance associated with using the aerocapture maneuver to slow high-mass systems from an Earth-approach trajectory into orbit around Mars. This work is done in conjunction with the Mars Entry Descent and Landing Systems Analysis (EDL-SA) task to explore candidate technologies necessary for development in order to land large-scale payloads on the surface of Mars. Among the technologies considered include hypersonic inflatable aerodynamic decelerators (HIADs) and rigid mid-lift to drag (L/D) aeroshells. Nominal aerocapture trajectories were developed for the mid-L/D aeroshell and two sizes of HIADs, and Monte Carlo analysis was completed to understand sensitivities to dispersions. Additionally, a study was completed in order to determine the size of the larger of the two HIADs which would maintain design constraints on peak heat rate and diameter. Results show that each of the three aeroshell designs studied is a viable option for landing high-mass payloads as none of the three exceed performance requirements.

Nomenclature

ΔV	=	change in velocity required post-aerocapture to achieve desired orbit
Φ	=	bank angle
ρ_0	=	reference atmospheric density
ρ_{est}	=	atmospheric density estimate
ρ_{mes}	=	measured atmospheric density
C_D	=	drag coefficient
C_L	=	lift coefficient
D	=	drag acceleration
D_{mes}	=	measured drag acceleration
D_{REF}	=	drag acceleration reference
g	=	gravitational acceleration
G_d	=	drag acceleration gain
G_h	=	altitude rate gain
h	=	altitude
h_0	=	reference altitude for density approximation
h_S	=	scale height for density approximation
$\dot{h}$	=	altitude rate
$\dot{h}_{ref}$	=	altitude rate reference
K_ρ	=	density multiplier
K	=	filter gain
m	=	mass

* Aerospace Engineer, Flight Mechanics and Trajectory Design Branch
† Aerospace Engineer, Flight Mechanics and Trajectory Design Branch, Senior Member AIAA
‡ Aerospace Engineer, Flight Mechanics and Trajectory Design Branch, Senior Member AIAA
§ Aerospace Engineer, Atmospheric Flight and Entry Systems Branch, Senior Member AIAA

Error! Bookmark not defined.Error! Bookmark not defined. $\bar{q}$ = dynamic pressure
R = radius
S = reference area
V_I = inertial velocity
V_{miss} = difference between predicted and desired exit velocity
V_r = relative velocity

I. Introduction

The Mars Entry, Descent, and Landing System Analysis (EDL-SA) project has been tasked with performing systems analysis to identify the optimal technologies required to land a 20-50 MT Exploration-class mission on Mars. It has been shown that it is not possible to safely land these large systems using heritage Mars EDL systems, or analogous Earth or Moon EDL systems. In 2007, NASA conducted a Mars Exploration Architecture[1] which included an in depth review of the science motivations and engineering technology requirements for a human Mars mission campaign. This study resulted in an update to the Mars Design Reference Architecture (DRA 5.0). Among the primary findings and recommendations was the conclusion that landing large payloads (greater than 1 MT) on the surface of Mars remains a key architectural challenge. Additionally, research and system studies of fundamental EDL technologies were highly recommended.

The EDL-SA project identified the candidate technologies and assembled them into full aerocapture and EDL sequences so that simulations could be developed to evaluate them. The chosen architectures, shown in Figure 1, combine the various technologies of interest in nine different ways. For aerocapture, three scenarios were considered. The first is a rigid mid-L/D aeroshell, which is represented in architectures 1, 4, 5, and 7. This scenario calls for a vehicle that flies at a 55-degree angle of attack, resulting in ballistic coefficient and L/D values of 490 kg/m^2 and 0.43, respectively. The second is a small-scale lifting hypersonic inflatable aerodynamic decelerator (HIAD), which is represented in architectures 2, 6, and 8. This scenario requires the vehicle to fly at a 22.2-degree angle of attack, which correlates to an L/D of 0.3 and was sized to provide a ballistic coefficient of 165 kg/m^2. Architecture 9, which was added later in the study, utilizes separate HIADs for both the aerocapture and EDL phases allowing the ballistic coefficient and L/D of the aerocapture HIAD to be tailored to meet the specific needs of that phase. This resulted in a much larger HIAD design sized to meet peak heat rate and diameter constraints, which resulted in an L/D and ballistic number of 0.2 and 33.33 kg/m^2, respectively. Architecture 3 is an all-propulsive sequence, and is not considered in this study. This narrows the number of aerocapture architectures down to 3: rigid mid-L/D aeroshell, small HIAD, and large HIAD.

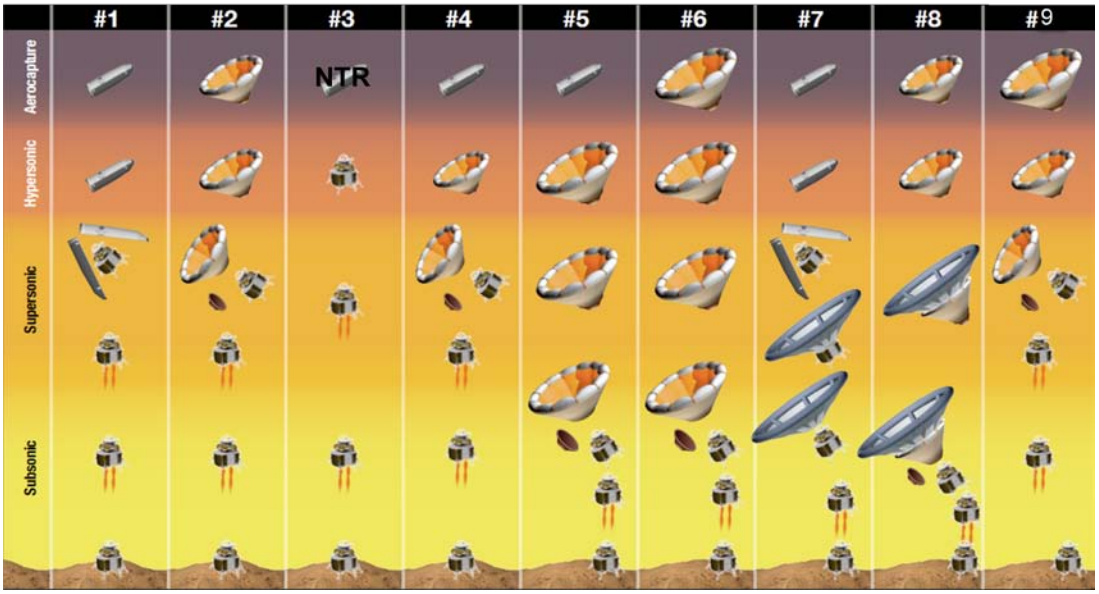

Figure 1. EDL-SA Architectures Diagram

For each configuration, Monte Carlo performance and sensitivity analysis were completed using the POST2 simulation at LaRC. This simulation uses the Hybrid Predictor Corrector Aerocapture Scheme (HYPAS) guidance algorithm to simulate the aerocapture phase.

II. The Aerocapture Maneuver

The purpose of aerocapture is to slow the vehicle from a hyperbolic velocity relative to the planet into an elliptical orbit around the desired landing body, prior to EDL. Figure 2 shows the aerocapture trajectory and highlights major events during the maneuver. The simulation used in this study utilizes the Hybrid Predictor Corrector Aerocapture Scheme (HYPAS)[2] guidance algorithm to simulate the bank modulation portion of the aerocapture phases. As shown in the figure, the vehicle enters the atmosphere (2) from a hyperbolic approach trajectory and begins bank angle modulation at a specific g-load trigger defined in the simulation. This marks the beginning of the first of the two aerocapture phases, the equilibrium glide phase. During this phase, the vehicle passes through orbit periapsis, and then transitions to the second phase, the exit phase, at a velocity trigger established in the simulation. Once the vehicle reaches another defined sense acceleration limit, bank angle modulation ceases, and the vehicle exits the atmospheres and coasts to the targeted orbit apoapsis. At the orbit apoapsis, a periapsis raise maneuver (9) is performed to raise the periapsis out of the atmosphere and avoid surface impact, and the vehicle coasts to its new orbit apoapsis. Here, a final orbit adjust maneuver (10) is performed to cleanup any errors associated with targeting during the aerocapture maneuver, and brings the vehicle into its desired post-aerocapture target orbit. Following a period of time in orbit, a de-orbit burn is performed in order to establish the desired atmospheric interface to initiate the EDL phase, which culminates with touchdown on the Martian surface.

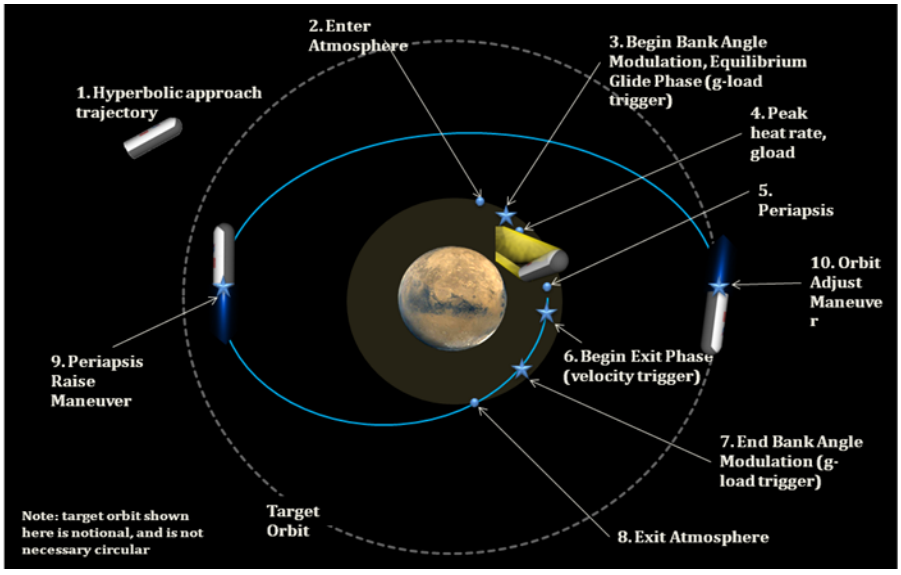

Figure 2. Aerocapture Phases

III. Aerocapture Simulation

The simulation used to evaluate the EDL-SA architectures is the Program to Optimize Simulated Trajectories (POST2)[3], which is a generalized point mass, discrete parameter targeting and optimization simulation. POST2 has the capability to target and optimize multiple vehicles near a rotating oblate planet and has extensive heritage for simulating ascent, descent, and orbiting trajectories including past missions like Shuttle, Stardust, Genesis, and Mars Missions such as Pathfinder, Odyssey Orbiter, Exploration Rovers, Reconnaissance Orbiter, and the Phoenix

Lander. POST2 is also used extensively in current missions like Mars Science Laboratory, Launch Abort Systems and Ares.

Specific models used to tailor production POST2 for the EDL-SA purposes include use of the Mars Global Reference Atmosphere Model 2005 (MarsGRAM 2005), a standard accepted throughout the field. The entry date was arbitrarily chosen to be November 3, 2010 (a MSL derivative), and the atmosphere entry altitude is approximately 125 km. The planet model included a gravitational constant equal to 4.2828376383e13 $kg*m^2/s^2$ with a mean equatorial radius equal to 3396190 m, a mean polar radius of 3376200 m and a planet rotation rate of 7.088218e-5 rad/sec. The gravity model included a JPL Mars 85x85 model truncated at 20x20, and the terrain model used $1/32^{nd}$ deg Mars Orbiter Laser Altimeter (MOLA) data. Other EDL-SA simulation specific models include aerodynamic and aerothermodynamic models for the HIAD and rigid mid-L/D aeroshell, and mass properties derived from response surface equations for HIAD and rigid mid-L/D aeroshell. In addition EDL-SA assumes that the trajectories have perfect Navigation knowledge.

The purpose of the first year of the EDL SA was to examine alternative architectures that would provide the aerocapture phase required by DRA5 for the cargo delivery vehicles. The approach velocity and target orbit were provided by DRA5, and to summarize, the hyperbolic approach velocity was set at 7.36 km/s and the target orbit was defined as 1Sol (33793km x 250 km). It was assumed for all the architectures that a reaction control system (RCS) would be the primary control, and to emulate the characteristics of a RCS without having to design a control system, a "pseudo-controller" was used where the bank acceleration, maximum bank rate, and bank direction are modeled.

IV. HYPAS Guidance

The HYPAS aerocapture guidance algorithm[4], developed at JSC, guides a lifting vehicle through the atmosphere to a desired exit orbit apoapsis and inclination using bank angle control. The guidance uses an analytically derived control algorithm based on deceleration due to drag and altitude rate error feedback, where inputs to the guidance algorithm are the current vehicle position, velocity, sensed acceleration, and body attitude. The algorithm outputs a commanded bank angle. The guidance algorithm is adaptable to a wide range of initial state vectors, vehicle lift-to-drag ratios and ballistic coefficients, planetary atmospheres, and target apoapsis and inclinations, by only changing a set of initialization constants. Furthermore, by tuning these constants[5], other trajectory constraints can be controlled such as maximum dynamic pressure, deceleration, heat rate, and the amount of the theoretical corridor captured.

A significant feature of the HYPAS algorithm is that no reference trajectories are computed prior to flight. All references are computed and updated during flight, and this analytic, "on-the-fly" approach leads to efficient code, minimal data storage requirements, and minimal preflight effort. The non-numerical, non-iterative scheme ensures fast and consistent execution times.

The original version of the HYPAS algorithm was developed for the Aeroassist Flight Experiment (AFE) program. During the AFE program, the algorithm was tested, compared, and evaluated against other guidance algorithms in three and six degree-of-freedom computer-based simulations. The HYPAS guidance algorithm was selected for the space flight test, and development of the flight code was on schedule until the AFE program was cancelled. Since the AFE program, the HYPAS algorithm has been used in numerous human and robotic exploration mission studies, and these studies involved developing nominal and dispersed trajectory simulation results for aerocapture at Earth, Mars, Titan and Neptune for a wide range of vehicle L/D, ballistic coefficients, entry conditions, and target orbits. HYPAS was also in the evaluation phase for the NASA/CNES 2005 Mars Sample Return Mission[6], which included an aerocapture orbiter at Mars. This work has provided the opportunity to gain a deep understanding of how the guidance algorithm performs in a variety of situations, and modifications have been made as necessary to improve performance and robustness.

The HYPAS guidance algorithm consists of two phases. In the first phase, or capture phase, bank angle commands are generated to stabilize the trajectory and drive the vehicle toward equilibrium glide conditions, where lift, gravity, and centripetal forces are balanced. When the vehicle decelerates to a specified velocity, the second phase, or exit phase, begins. In the exit phase, the velocity vector at atmospheric exit altitude is analytically predicted each guidance computation cycle. Bank angle commands are then generated so that the velocity achieved at exit altitude will produce an orbit with the target apoapsis. This two-phase approach allows separate tuning of initialization constants to maximize robustness during capture and maximize performance during exit.

Additionally, because bank modulation is used to control both drag and inclination angle, a natural division is created in the logic between in-plane or longitudinal control, and out-of-plane or lateral control. The longitudinal control commands the vehicle to a specific bank angle magnitude, thereby controlling the amount of vertical in-plane lift. The lateral control commands the sign of the bank angle, which controls the direction of the out-of-plane lift, in order to maintain the desired orbit inclination within a deadband by performing roll reversals.

The longitudinal control is tasked with ensuring the vehicle exits the atmosphere with the velocity and flight path angle required to meet to the desired target orbit apoapsis. Target apoapsis is achieved by controlling the vertical component of the lift vector through bank angle commands. The guidance algorithm follows a reference altitude rate and drag profile, generating bank angle commands using the control equation

(1)

where Φ_{cmd} is the commanded bank angle, $\dot{h}$ is the altitude rate, $\bar{q}$ is the dynamic pressure, D is the deceleration due to drag, and $\Phi_{eq.gl.}$ is the bank angle required for equilibrium glide. $G_{\dot{h}}$ and G_d are gains selected to provide the desired natural frequency and damping ratio response to a second order differential equation in altitude. Their values can be adjusted to maximize performance or robustness.

During the capture phase, when equilibrium glide is targeted, the reference altitude rate, $\dot{h}_{ref}$, is zero, and the reference drag is computed each time step by

(2)

where V_I is current inertial velocity, R is current radius vector magnitude, g is acceleration due to gravity, C_L and C_D are lift and drag coefficients, and K is a factor to determine how much of the lift vector should be used to maintain equilibrium glide. The guidance will attempt to ensure the vehicle will not skip out by balancing the vertical forces. Selection of the gains controls the point in the entry in which equilibrium glide is established, thereby controlling heat rate and g-loads.

During the exit phase of the guidance, a constant reference altitude rate is computed so that the velocity at atmospheric exit will provide the desired target apoapsis altitude. This reference altitude rate is updated each guidance cycle based on the difference between the predicted and desired exit velocity. The equation for updating the reference altitude rate is

(3)

where V_{miss} is the difference between the predicted velocity at exit and the velocity required at exit to achieve the apoapsis target with given reference altitude rate. The predicted exit velocity is computed from an analytic equation that assumes an exponential atmosphere and constant radial velocity to atmosphere exit for estimating velocity loss due to drag. The desired exit velocity is simply computed from orbital mechanics equations.

The guidance algorithm requires an estimate of the current atmospheric density, which is derived from the measured deceleration due to drag assuming a nominal ballistic coefficient using

(4)

where V_r is the current relative velocity, and D_{mes} is the sensed deceleration due to drag. The guidance algorithm models the atmosphere density as a simple exponential law of altitude

(5)

where r_0, and h_0, are the reference density and altitude, and h_s is the scale height. A density scale multiplier K_ρ is defined as the ratio of the density expected from the exponential model and the measured density. A first order low-pass filter of the form

(6)

is used to smooth high-frequency atmosphere disturbances and control the guidance response rate to density changes. Then, the estimate of the atmosphere density is computed by

(7)

Note that with this approach, the guidance algorithm automatically compensates for dispersions in both atmospheric density and vehicle drag coefficient.

The lateral control is tasked with achieving the target orbit inclination by performing periodic bank reversals. The logic in the guidance algorithm uses an inclination or wedge angle dead band that is a function of inertial velocity. Whenever the inclination or wedge angle error exceeds this dead band, a roll reversal is commanded. The direction to bank is selected through a series of tests that examine current velocity, angular distance to roll, and difference between reference and navigated altitude rate.

V. Results

1. *Aerocapture Flight Path Corridor Sizing*

Initially, the theoretical lift up-lift down profile was flown, in place of HYPAS, to gain an understanding of the expected performance for the three aeroshell designs. Performance can be evaluated based on the available skip-out margin which is defined as the difference between the flight path angle flown for an individual case and the flight path angle that causes skip-out. Logically, the more skip-out margin the better the performance observed in the Monte Carlo analysis. Figure 3 shows the skip-out margin for a range of ballistic numbers and L/D values. The flight path angle is chosen such that the maximum g-load is 4-earth g's. The figure also highlights the three aeroshell designs studied in this analysis according to each design's L/D and ballistic number combination and shows the amount of skip-out margin available for each design. Analysis has shown that a minimum skip-out margin of 1 degree is required for good performance (i.e. no cases lost to skip-out) in the Monte Carlo runs. The 23 meter diameter inflatable aeroshell has 1.25 degrees, the 55 meter diameter inflatable aeroshell has roughly 0.9 degrees, and the rigid mid-L/D aeroshell has approximately 1.6 degrees. Therefore, good performance is expected from Monte Carlo analysis for both the 23m HIAD and rigid mid-L/D aeroshell, however, not for the 55 meter HIAD.

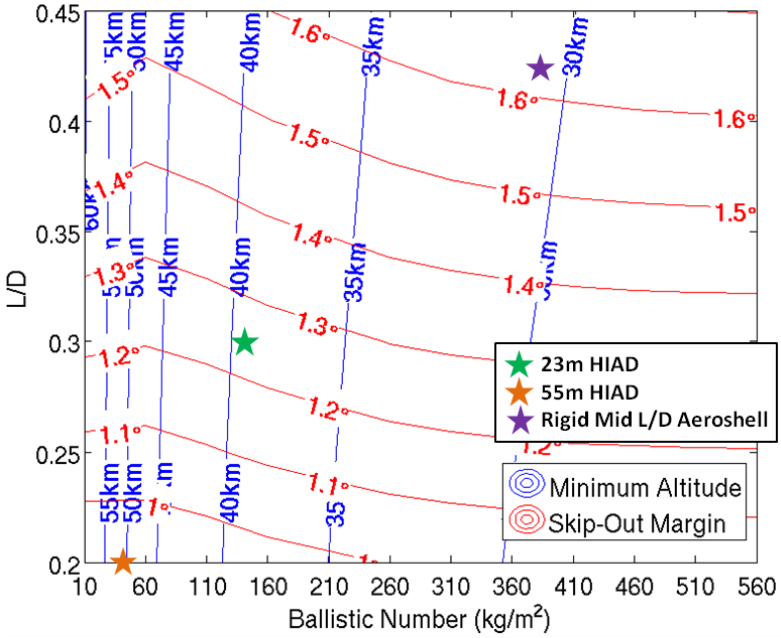

Figure 3. Available Skip-out Margin for Variations of L/D and Ballistic Number

2. Nominal Trajectory Results

Reference trajectories were developed for the three different aeroshells using a 1 sol (33793 km x 250 km) post-aerocapture target orbit, and for each of these references, the HYPAS analytical closed-loop guidance algorithm was used to generate the trajectories. For each aeroshell design, the flight path angle at entry interface was chosen to meet the desired peak g-load of 3 earth-g's for each case.

Figure 4 compares the altitude profiles for each of the three configurations studied, and shows that the minimum altitude decreases as the ballistic number increases. The 55 m HIAD has the lowest ballistic number, and reaches a minimum altitude just below 50 km. Conversely, the rigid mid-L/D aeroshell is the highest ballistic number and reaches a minimum altitude of slightly higher than 30 km.

Figures 5 and 6 show an example of the key trajectory guidance parameters using the 23 m HIAD nominal trajectory. These parameters include bank, drag acceleration, and altitude rate. The bank profile, which the guidance algorithm commands in order to fly the drag acceleration and altitude rate reference profiles, shows good performance in that the bank is consistently being modulated and does not saturate the guidance by holding full lift up (0 degrees) or full lift down (180 degrees) during the guided portion of the maneuver. Additionally, the drag acceleration and altitude rate profiles follow their reference profiles as expected. The drag acceleration is trying to pull the vehicle deeper into the atmosphere in order to avoid skip-out, whereas the altitude rate is attempting to maintain the equilibrium glide condition of constantly increasing altitude. However, the actual trajectory does not match the reference profiles exactly, as each profile is attempting to achieve competing objectives. Similar nominal trajectory data was generated for the 55 m HIAD and rigid mid-L/D aeroshell cases.

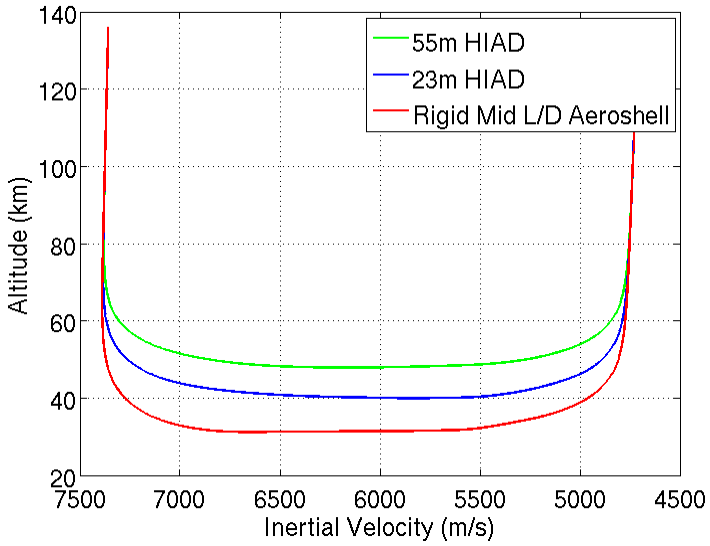

Figure 4. Altitude Profiles for All Configurations

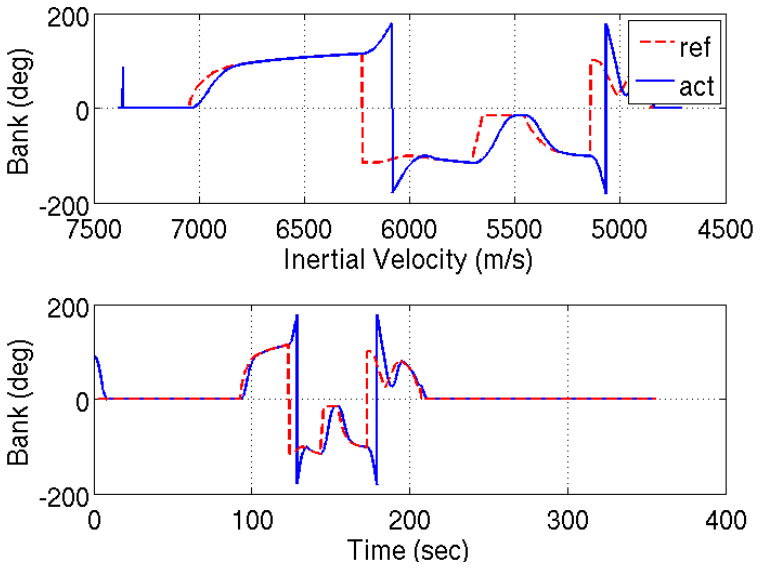

Figure 5. Nominal Bank Profiles for the 23 m HIAD

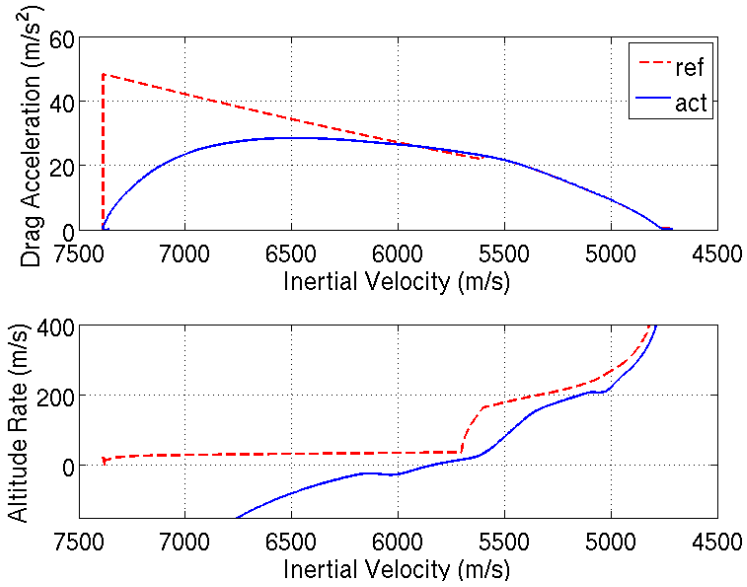

Figure 6. Nominal Drag Acceleration and Attitude Rate Profile for 23 m HIAD

3. Monte Carlo Results

Sets of 2000 case Monte Carlo runs were completed for each of the three reference profiles, and the HYPAS gains were optimized for ΔV performance within each set. The applied dispersions[7] are listed in Table 1.

Table 1. Aerocapture Monte Carlo Dispersion Values

Dispersion	Value
Aero	+/- 10% (normal, 3σ)
Alpha	+/- 5% (normal, 3σ)
Entry Flight Path Angle (EFPA)	+/- 0.35° (normal, 3σ)
Dust Tau	0.1:0.9 + random density perturbations
Mass	+/- 5% (normal, 3σ)

Figures 7 through Figure 1 display key Monte Carlo results for each of the three aeroshell designs considered in this study. The figures are shown in order of decreasing ballistic number and L/D, with the rigid mid-L/D aeroshell having the highest combination of the two, and the 55m HIAD having the lowest. With the exception of one extraneous high point in the rigid mid L/D Monte Carlo results, it is observed that as ballistic number and L/D decreases, the range of apoapse altitude reached and the amount of ΔV required to perform the post aerocapture clean up burn increases. There is a direct correlation between the size of the apoapse altitude target miss distance and the amount of ΔV required to clean up that miss. The larger the miss distance, the larger the clean up burn must be to put the vehicle into the target 1 sol orbit.

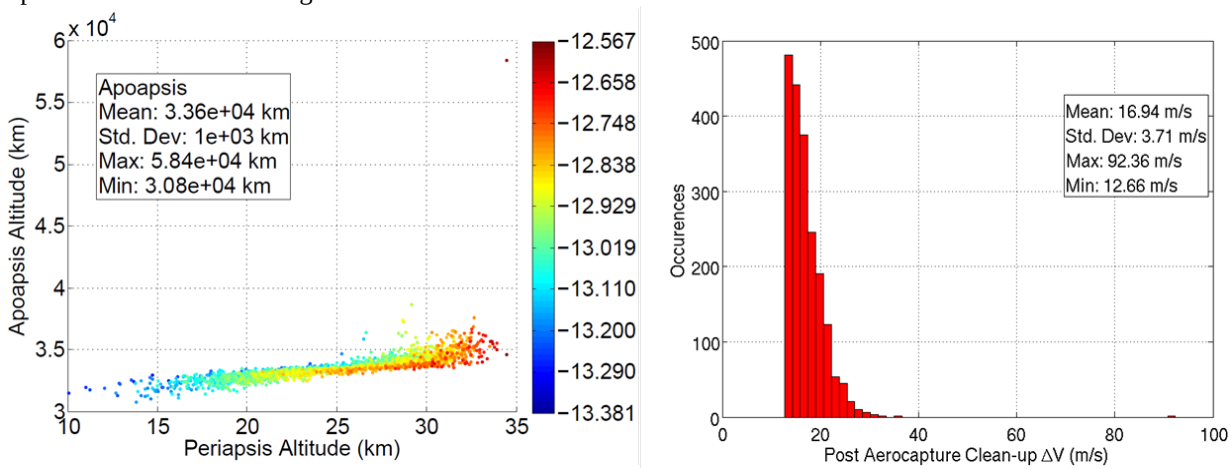

Figure 7. Monte Carlo Results for the Rigid Mid-L/D aeroshell

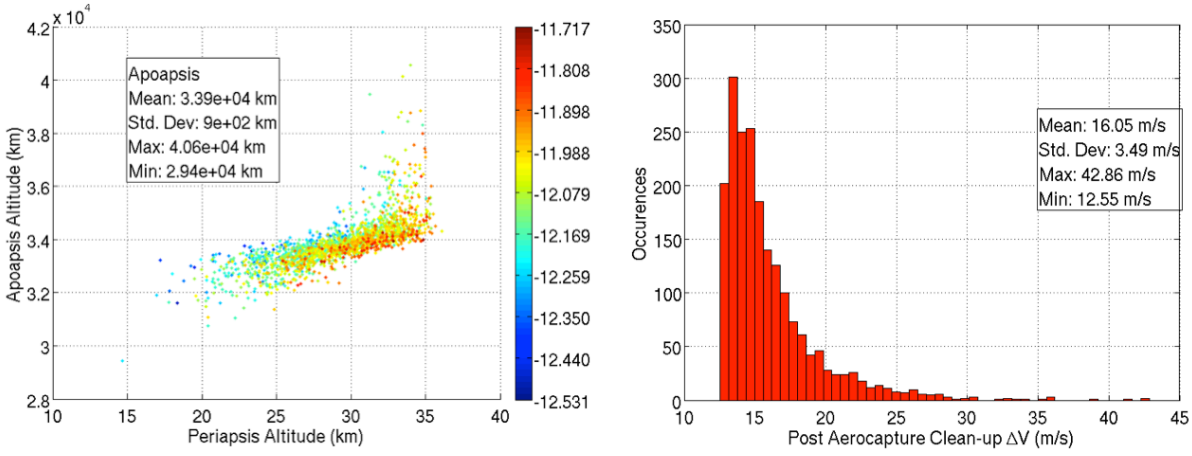

Figure 8. Monte Carlo Results for the 23 m HIAD, L/D = 0.3

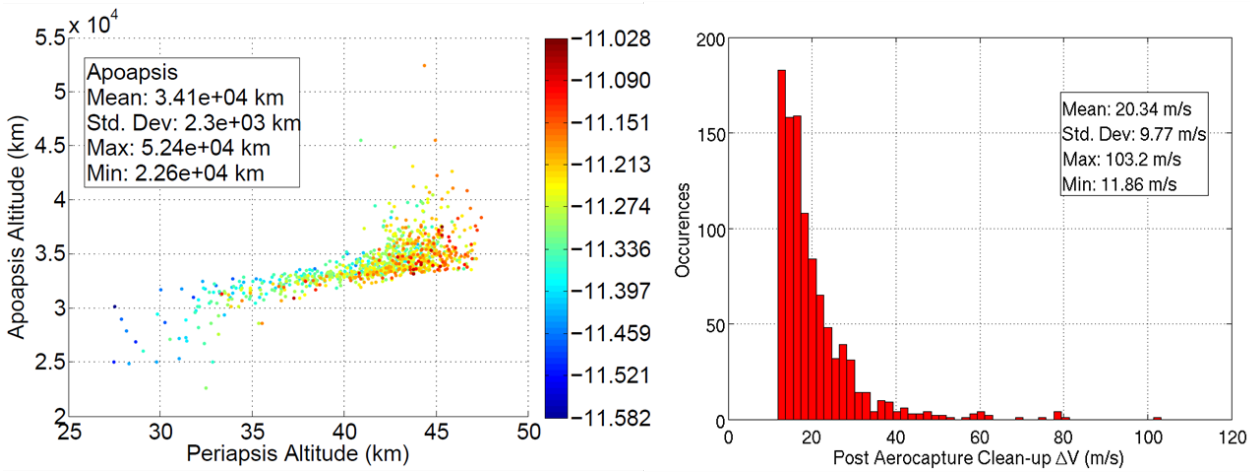

Figure 1. Monte Carlo Results for the 55 m HIAD, L/D = 0.2

The single high apoapse altitude of 58,400 km observed in the rigid mid-L/D aeroshell results in Figure 7 is attributed to poor tuning in the guidance gains. With improved guidance tuning, the maximum ΔV value for that design could be brought below the maximum ΔV observed in the 23m HIAD and 55m HIAD cases, as both the 23m HIAD and 55m HIAD cases are well tuned, and the performance observed is ideal.

The increasing trend in larger apoapse altitude misses and higher associated ΔV values from the rigid mid-L/D aeroshell to the 55m HIAD can be attributed to a decrease in L/D value. As stated previously, the larger the apoapse altitude miss, the larger the clean-up burn required to correct the miss. The lower the L/D, the less lift the vehicle is able to command throughout the guided portion, which increases the difficulty the guidance has in achieving the target altitude rate profile. This, coupled with the worst of the Monte Carlo dispersions, creates individual cases in which the guidance, commanding the maximum amount of lift, is still unable to meet the altitude rate targets and exits the atmosphere with a large apoapsis altitude error. Though less than ideal performance is observed in Figure 1 for the L/D=0.2 case, the required ΔV is still below the budgeted 150 m/s, therefore, the performance is deemed acceptable.

4. Sensitivities

After evaluating the performance of each of the three vehicle designs in the Monte Carlo analysis, several sensitivity studies were also performed to evaluate the effect of additional parameter changes on the post aerocapture clean up ΔV. Nominal trajectories were simulated with parametrically varied atmosphere inputs such as season, dust opacity, and time of day over the full or expected range, as well as the initial mass and target orbit. Gain scaling (but not tuning) was performed for the mass sensitivity cases, and no gain changes were made for the atmosphere sensitivities. An examination of the results of atmosphere and mass sensitivities resulted in no significant variation (less than 8 m/s) or trends in variation of ΔV primarily because of vehicle velocity and the fact that the guidance is capable of flying out the variations. That was not the case for the sensitivity study that considered various target orbits.

The choice of target orbit, or post aerocapture apoapsis altitude (ranging from 33,793 km to 500 km) was determined to have a significant effect on the ΔV required for the post-aerocapture cleanup maneuver. Figure 10 shows the cleanup ΔV that results from the sensitivity that compared the aerocapture of a 23m HIAD vehicle into both a 1 sol and 500 km circular post-aerocapture target orbit. A significant difference in mean ΔV, roughly 100 m/s, is observed, showing that while the vehicle may not be sensitive to variations in mass or atmosphere inputs, it is highly sensitive to changes in the post-aerocapture target orbit.

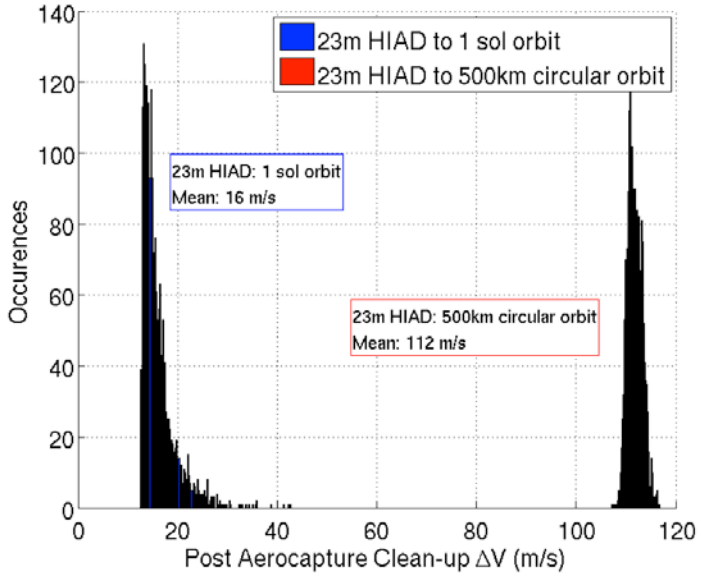

Figure 10. Delta V Sensitivity to Post-Aerocapture Orbit

5. Breakpoint Study Trade

Initially, the study called for the analysis of only two vehicle designs, the small 23 m HIAD and the rigid mid-L/D aeroshell. The 23m HIAD design sees a high enough heat rate such that an ablative TPS is required. An additional study was undertaken to determine the HIAD size at which the heat rate would go below 50 W/cm^2, which is a low enough heat rate such that an insulating TPS could potentially be used. Additionally, it was desired to understand at how low an L/D it would become difficult to perform an aerocapture.

The range of L/D and ballistic numbers considered for the study were 0.1 to 0.3 and 25 to 50 kg/m^2, respectively. Sixteen specific combinations of L/D and ballistic numbers were created from these ranges and considered for a scaled HIAD aeroshell configuration that aerocaptured into a 1sol orbit. Results show that performance is highly sensitive to L/D, and that poor performance is observed for L/D's less than 0.25.

Revisiting the concept of skip-out margin and understanding the amount available for each combination provided insight into aerocapture performance that would be observed in the Monte Carlo analysis. Figure 11 shows the skip-out margin available for the 16 combinations considered, and the figure shows that for L/D values less than 0.25, the amount of skip-out margin is less than the previously discussed one-degree required to obtain sufficient performance.

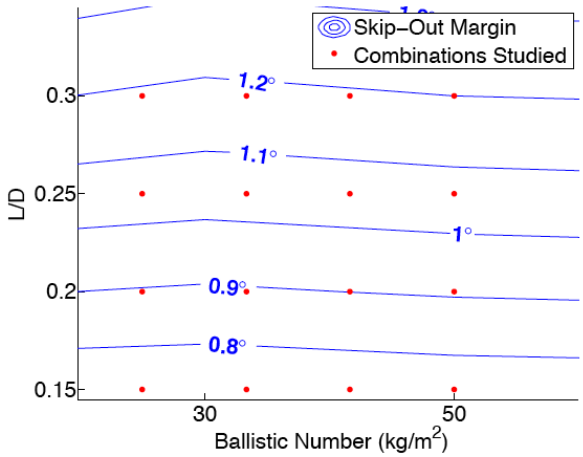

Figure 11. Available Skip-out Margin for Low Combinations of L/D and Ballistic Number

Using well tuned guidance gains for one high L/D and ballistic number combination, the gains were scaled down, but not individually tuned, and 2000 case Monte Carlo simulations were performed for each of the sixteen combinations. Figure 12 shows the post aerocapture ΔV range required to target a 1 sol orbit for each of the combinations, relative to the 150 m/s of budgeted ΔV.

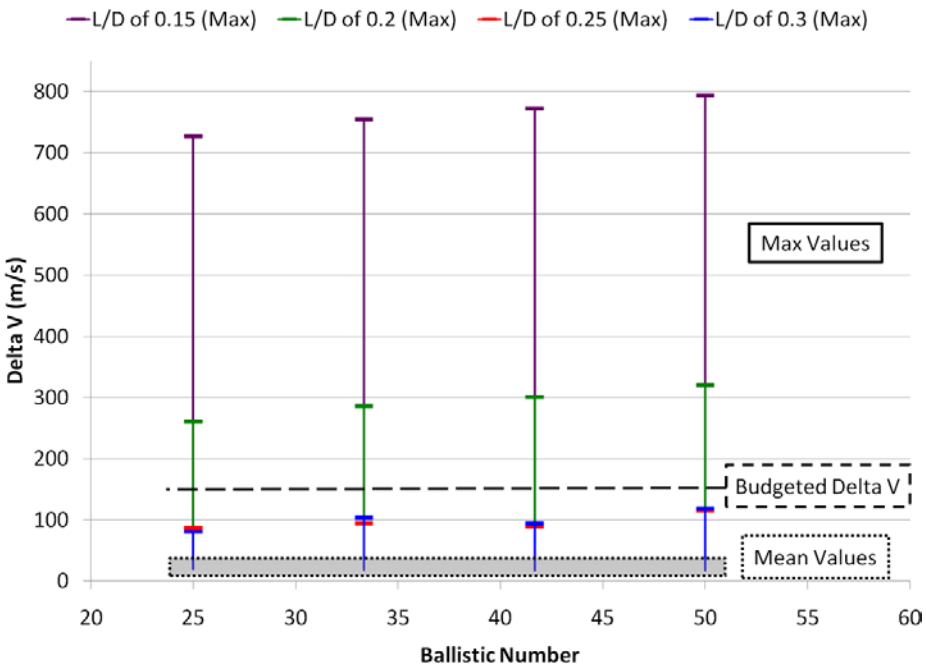

Figure 12. ΔV Monte Carlo Results

The key parameter to note is the maximum ΔV value required to clean up large apoapsis miss distance for each value of L/D. Validating known poor performance at low skip out margins, the L/D=0.15 data has several cases that require more than 700 m/s of clean up ΔV, significantly exceeding the budgeted amount of 150 m/s. Even for an L/D=0.2, 300 m/s of ΔV is required, exceeding the budgeted amount, while the cases with L/D=0.25 and L/D=0.3 show acceptable performance by remaining below budget. Therefore, the "break point" of the simulation would be L/D values of 0.20 and lower, which show unacceptable performance in terms of ΔV.

In terms of selecting a suitable ballistic number, Figure 13 shows the relationship between the Monte Carlo 3-σ peak heat rate values and HIAD diameter. Each line represents a different value of L/D, which is shown to have a relatively small effect on the peak heat rate. The data also shows that the choice of HIAD diameter (or the effect of ballistic coefficient) has a significant effect on the peak heat rate.

Initial mass and aerodynamic models limited the HIAD diameter to 50 m, and the breakpoint study considered that holding to a 3-σ peak heat rate of less than 50 W/cm^2 in the Monte Carlo analysis would enable use of the same models by maintaining diameters below 50 m. Based on results shown in Figure 13, it is clear that no combination of ballistic number and L/D considered for the break point study is sufficient to meet both the 50 W/cm^2 peak heat rate and 50m diameter constraints. Meeting the heating constraint was considered more important than meeting the diameter constraint; therefore, the HIAD diameter was allowed to increase to 55 m, which corresponds to a ballistic number of 33.33 kg/m^2. Consequently, only a ballistic number of 33.33 kg/m^2 and 41.67 kg/m^2, which is the next closest to meeting both the HIAD and peak heat rate constraints, can be considered viable options for this design.

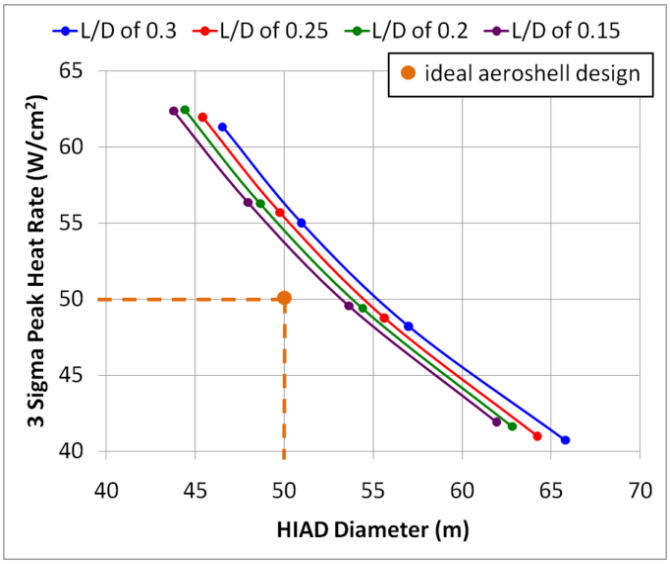

Figure 13. Plot of 3 sigma peak heat rate versus diameter for lines of constant L/D

The previous data includes dispersed results for a scaled, but un-tuned set of guidance gains. The next step in characterizing the breakpoint was to choose a breakpoint set of cases for which to tune gains to examine improvements in performance. Gain tuning is a labor intensive process, so only 4 of the 16 cases were selected for tuning. From the analysis displayed in Figures 12 and 13, it appears that L/D is the driver in ΔV meeting requirements, and ballistic number in meeting peak heat rate and diameter requirements. Therefore, the two L/D (0.15 and 0.20) and ballistic number (33.33 kg/m^2 and 41.67 kg/m^2) breakpoints determined from Figures 12 and 13 were combined to form the four combinations to be optimized using guidance gain tuning.

An additional change implemented at this time was a reduction of the entry flight path angle dispersion to 0.25 deg. The Mars Approach Navigation community felt that the previous value of 0.35 deg was overly conservative, and that a reduction to 0.25 deg is more appropriate while still being sufficiently conservative. The results of this modification for the optimized L/D = 0.2, ballistic number of 33.33 kg/m^2 (or 55 m diameter) case are shown in Figure 2. The effect of reducing the flight path angle dispersion and optimizing the guidance tuning resulted in a maximum ΔV below the budgeted 150 m/s, deeming this combination to have acceptable performance. One stray case, highlighted in red, can be attributed to imperfect tuning of the guidance gains.

L/D=0.15 cases (not shown) still remained almost 400 m/s over the budget, therefore, L/D=0.2 was determined to be the breakpoint in L/D. The final ballistic number breakpoint was selected as 33.33 kg/m^2, which corresponds to the 55 m HIAD. In summary, the breakpoint of the aerocapture simulation using the HYPAS guidance algorithm was determined to be for cases below an L/D of 0.2 and ballistic number of 33.33, and this combination was carried through in the design of the large 55m HIAD.

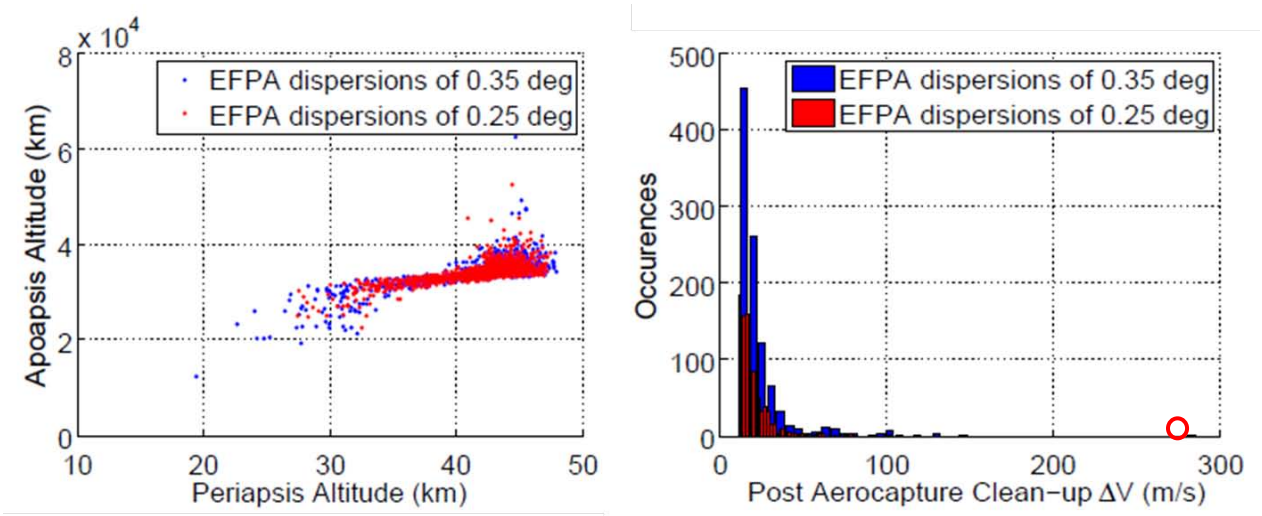

Figure 2. Effect of Flight Path Angle Dispersions for L/D=0.2, Bn=33.33 kg/m^2

VI. Conclusion

In summary, three aeroshell concepts designed for high-mass payloads were analyzed in the POST2 simulation to understand the performance of the aerocapture guidance. The three concepts were created from two of the candidate technologies identified by the Mars Entry Descent and Landing System Analysis project, and are the rigid mid-L/D aeroshell and the hypersonic inflatable aerodynamic decelerator. For each aeroshell design, a nominal trajectory was developed and Monte Carlo analysis was performed from those nominal trajectories to determine if any of the three designs exceeded performance requirements. In this analysis, minimum performance requirements dictate that each of the three designs should consume no more than 150 m/s of ΔV during the aerocapture maneuver.

In each of the three concepts, no single aeroshell design required more than 150 m/s of ΔV, therefore each of the three designs is considered a viable option for landing high-mass payloads. It was observed, however, that the sensitivity to Monte Carlo dispersions increased as the L/D of the vehicle decreased, showing a larger miss in the target orbit apoapsis and a corresponding larger clean-up ΔV. Additionally, the analysis showed extreme sensitivity to a change in post-aerocapture target orbit. Both of these aspects should be considered in future aeroshell and aerocapture mission design.

Acknowledgments

The authors of this paper would like to acknowledge the contributions of the EDL-SA team. In particular, Richard Powell, Jeremy Shidner, and Jody Davis were instrumental in developing the simulation, answering POST2 questions, and reviewing these results. This work would not be possible without their efforts.

References

[1] B.G. Drake (ed.), Human Exploration of Mars Design Reference Architecture 5.0, NASA-SP-2009-566, July 2009

[2] Cerimele, C., Gamble, J. "A Simplified Guidance Algorithm for Lifting Aeroassist Orbital Transfer Vehicles." AIAA-85-0348, AIAA 23rd Aerospace Sciences Meeting, Reno, Nevada, January 1985

[3] Powell, R. W., Striepe, S. A., Desai, P. N., Queen, E. M., Tartabini, P. V., Brauer, G.L., Cornick, D. E., Olson, D. W., Petersen, F. M., Stevenson, R., Engle, M. C., Marsh, S. M., "Program to Optimize Simulated Trajectories (POST2), Vol. II Utilization Manual." Version 1.1.1G, May 2000, NASA Langley Research Center, Hampton VA

[4] Bryant, L., Tigges, M., Ives, D., "Analytic Drag Control for Precision Landing and Aerocapture." AIAA-98-4572, AIAA Atmospheric Flight Mechanics Conference, Boston, MA, August 1998.

[5] McCleary, B., Westhelle, C., "Analytic Predictor-Corrector Aerocapture Guidance Tuning Procedure." EG-DIV-05-1, November 2005, NASA Johnson Space Center, Houston TX

[6] Masciarelli, J., Rousseau, S., Fraysse, H., Perot, E. "An Analytic Aerocapture Guidance Algorithm for the Mars Sample Return Orbiter." AIAA-2000-4116, AIAA Atmospheric Flight Mechanics Conference, Denver, CO, August 2000.

[7] Report of the Design Reference Missions, Ground Rules and Assumptions, and Figures of Merit, EDLSA-001 Rev A, Sept. 1, 2009